Tuning the magnetocaloric response in half-Heusler/Heusler $MnNi_{1+x}Sb$ solid solutions

Emily E. Levin,* Joshua D. Bocarsly, Kira E. Wyckoff, Tresa M. Pollock, and Ram Seshadri
Materials Department, University of California, Santa Barbara, California 93106, USA and
Materials Research Laboratory, University of California, Santa Barbara, California 93106, USA
(Dated: November 30, 2017)

Materials with a large magnetocaloric response are associated with a temperature change upon the application of a magnetic field, and are of interest for applications in magnetic refrigeration and thermomagnetic power generation. The usual metric of this response is the gravimetric isothermal entropy change ΔS_M. The use of a simple proxy for the ΔS_M that is based on density functional theory (DFT) calculations of the magnetic electronic structure, suggests that half-Heusler MnNiSb should be a better magnetocaloric than the corresponding Heusler compound $MnNi_2Sb$. Guided by this observation, we present a study of $MnNi_{1+x}Sb$ ($x = 0$, 0.25, 0.5, 0.75, 1.0) to evaluate relevant structural and magnetic properties. DFT stability calculations suggest that the addition of Ni takes place at a symmetrically distinct Ni site in the half-Heusler structure, and support the observation using synchrotron X-ray diffraction of a homogeneous solid solution between the half-Heusler and Heusler endmembers. There is a maximum in the saturation magnetization at $x = 0.5$, and the Curie temperature systematically decreases with increasing x. ΔS_M for a maximum magnetic field change of $\Delta H = 5\,\mathrm{T}$ monotonically decreases in magnitude from $-2.93\,\mathrm{J\,kg^{-1}\,K^{-1}}$ in the half-Heusler to $-1.35\,\mathrm{J\,kg^{-1}\,K^{-1}}$ in the Heusler compound. The concurrent broadening of the magnetic transition results in a maximum in the refrigerant capacity at $x = 0.75$. The Curie temperature of this system is highly tunable between 350 K and 750 K, making it ideal for low grade waste heat recovery *via* thermomagnetic power generation. The increase in ΔS_M with decreasing x may be extendable to other $MnNi_2Z$ Heusler systems that are currently under investigation for use in magnetocaloric refrigeration applications.

INTRODUCTION

The need for energy-efficient and environmentally friendly technologies has prompted research into materials for efficient magnetic refrigeration and thermomagnetic power generation. These technologies rely on the magnetocaloric effect (MCE), which is the reversible change in temperature of a material upon a change in applied magnetic field. In a typical ferromagnet near its magnetic transition temperature, the adiabatic application of a magnetic field causes the entropy of the spin system to decrease as spins order in the direction of the applied field. Because entropy must be conserved in an adiabatic process, the lattice entropy, and therefore temperature, increases, causing the magnetocaloric effect. By alternating adiabatic and isothermal magnetization and demagnetization, this phenomenon can be be used to drive a thermodynamic cycle.[1] Magnetic refrigeration technology is expected to be very energy-efficient, and eliminates the need for harmful refrigerants, such as hydrochlorofluorocarbons, further proving to be an environmentally friendly option.

The magnetic transition temperature of a magnetocaloric material determines its applicability. Of primary interest are materials with transitions near room temperature, which can be used for residential and commercial refrigeration.[1,2] Materials displaying a large magnetocaloric effect at high temperatures may have uses in recovery of waste heat *via* thermomagnetic power generation, while low temperature materials may be used for gas liquefaction.[3,4] There is currently a lack of information on the magnetocaloric properties of materials with transition temperatures above room temperature, which is a hindrance to the study of thermomagnetic generators for waste heat recovery.

The temperature change $\Delta T_{ad}(H,T)$ in a material upon adiabatic application of a magnetic field H, and the isothermal change in entropy $\Delta S_M(H,T)$ upon application of a field, are used to describe the magnetocaloric effect in a specific material. While measuring ΔT_{ad} requires specialized equipment, ΔS_M can be calculated from straightforward magnetic measurements, discussed later.

ΔS_M is dependent on the slope of the magnetization *vs.* temperature curve, and so a peak in ΔS_M will occur at the ferromagnetic to paramagnetic transition, or the Curie temperature (T_C). The magnitude of ΔS_M is dependent both on the magnetization of the material, and on the breadth of the transition. Materials with first-order magnetic phase transitions[5] tend to have a very sharp transition, and therefore a high ΔS_M over a small temperature range, but thermal and magnetic hysteresis can cause intrinsic irreversibilities which reduce cooling efficiency.[6,7] Materials with standard second-order magnetic ferromagnetic to paramagnetic transitions, on the other hand, tend to have lower values of ΔS_M over a larger temperature range, and are free from these irreversibility losses.

Heusler and half-Heusler compounds, which crystallize in the $Fm\bar{3}m$ and $F\bar{4}3m$ structures respectively, as shown in Figure 1, are well-known for a wide variety of exotic functional magnetic properties, including half-metallic ferromagnetism,[8,9] magnetic shape memory,[10–12] and magnetocaloric behavior.[13–16] Heuslers, which have the stoichiometry XY_2Z, are comprised of four interpenetrating fcc sublattices, such that the X and Z atoms form a rock salt lattice and the Y

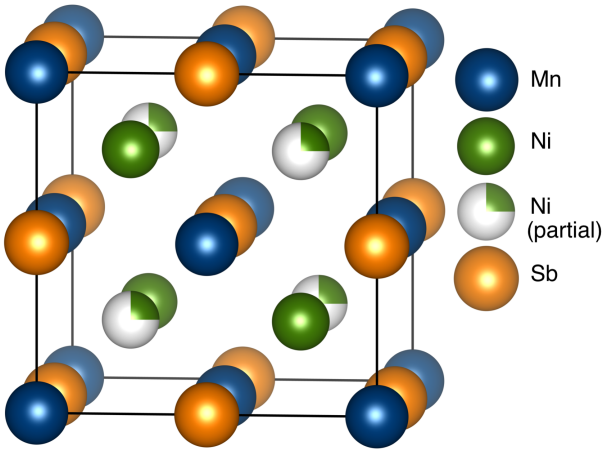

FIG. 1. Crystal structure of the solid solution $MnNi_{1+x}Sb$. The half-Heusler XYZ with the space group $F\bar{4}3m$ corresponds to one of the Ni sublattices being vacant, while the Heusler XY_2Z in the $Fm\bar{3}m$ space group corresponds to completely occupied sublattices, with only one symmetrically distinct nickel site. As nickel is added to the half-Heusler, the second Ni sublattice becomes partially occupied, as shown.

atoms occupy the tetrahedral voids in the rock salt lattice. In half-Heuslers, one of the Y sublattices is vacant, leaving only half of the tetrahedral sites occupied.

The magnetocaloric effect in $MnNi_2Z$ (Z = Sb, Sn, In, Ga) Heusler compounds has been studied extensively due to the coupled structural and magnetic transitions that can be found in materials with off-stoichiometric compositions.[16–19] These first order magnetostructural transitions lead to a large entropy change, but face problems with the intrinsic irreversibility and thermal hysteresis. For this reason, much research has focused on narrowing thermal hysteresis and operating within a minor loop of the hysteresis, where only a partial conversion between phases is performed.[6,19–21] The phase transition involves a significant volume change, which poses a challenge for engineering a device that must withstand continuous, rapid cycling.[2,22]

This challenge was acknowledged by Singh *et al.*, who explored the system $Mn_{1+x}Ni_2In_{1-x}$ ($x < 0.4$) aiming to increase ΔS_M by increasing magnetization without driving a first-order transition. As x increases, some of the Z site is replaced by Mn, increasing the overall moment and leading to an improved ΔS_M.[7] In $MnNi_2Z$ Heusler systems, ferromagnetic exchange between Mn atoms, which provide the most significant contribution to the magnetization, is mediated by Ni atoms on the Y site. Substitution of Mn on the Z site will result in ferromagnetic coupling, as both will have mutual parallel coupling to the Ni. Substitution of Mn on the Y site, on the other hand, results in antiferromagnetic coupling between Mn atoms, as no Ni is mediating the exchange, resulting in lowering the magnetization. Substituting Mn on the Z site or decreasing the nickel occupancy on the Y site, as shown in this contribution, are two techniques to increase net magnetization and yield larger ΔS_M. However, the Mn:Ni anti-site disorder present in Heuslers implies a preference of Mn to sit on the Y site, which will likely not allow both techniques to be used simultaneously.[23,24]

The magnetic deformation Σ_M, a density functional theory (DFT) based proxy developed by Bocarsly *et al.*, is a measure of the unit cell deformation between relaxed structures with and without the inclusion of spin polarization.[25] Σ_M is an indication of the coupling between magnetism and structure, and it correlates well with ΔS_M. In the solid solution between MnNiSb and $MnNi_2Sb$, the half-Heusler has a larger Σ_M (1.61%) than the full-Heusler (1.21%), and so we expect to have a larger $|\Delta S_M|$ as Ni content decreases. Experimental results in this study agree, supporting the importance of the coupling between magnetism and structure to the magnetocaloric effect.

The half-Heusler MnNiSb is well known as the first predicted half metal by de Groot *et al.* in 1989.[8] It possesses 100% spin polarization at the Fermi level due to a gap in the minority spin density of states. Its high Curie temperature (754 K), large magnetization (3.93 μ_B/f.u.), and spin polarization make it an ideal candidate for spintronics.[26,27] However, the Curie temperature is too high to be useful as a room temperature magnetic refrigeration material, and is above the range needed for the conversion of low grade waste heat by thermomagnetic generation.

It has been shown in previous studies that a maximum in the saturation magnetization exists at an intermediate composition in $MnNi_{1+x}Sb$ ($0 \leq x \leq 1$), and the Curie temperature can be varied between 750 K and 350 K.[27,28] The maximum in M_S suggests that removing nickel from the Heusler could increase $|\Delta S_M|$ while allowing for a tunable transition temperature useful for thermomagnetic power generation using low ($\leq$ 505 K) and medium grade (505 K to 923 K) waste heat.[3] In the present contribution, the magnetocaloric effect in the series $MnNi_{1+x}Sb$ is characterized. The magnitude of ΔS_M decreases with increasing nickel content, while the refrigerant capacity (RC_{FWHM}), a measure of the heat that may be transferred between the hot and cold reservoirs, is maximized for the $x = 0.75$ composition.[2] Here, we demonstrate a materials system with significant ΔS_M over a large range of transition temperatures useful for thermomagnetic power generation. These results may prove useful in other well-studied Heusler systems which behave similarly.

METHODS

Polycrystalline samples of $MnNi_{1+x}Sb$ (x = 0, 0.25, 0.5, 0.75, 1.0) were prepared *via* a rapid and energy efficient susceptor-assisted microwave technique.[29,30] Stoichiometric amounts of elemental powders were ground together (10 min.), pressed into a pellet, and sealed in an

evacuated fused silica ampoule. The ampoule was placed in a crucible with 7 g activated charcoal (DARCO 12-20 mesh), which was placed in an alumina foam housing in a 1200 W Panasonic domestic microwave oven (model NN-SN651B). Samples were reacted at 70% power for 2.5 minutes, and then reground for 10 minutes to ensure homogeneity. The powders were again pressed into a pellet and then annealed under vacuum at 923 K for 7 days before quenching in air.

Powder synchrotron X-ray diffraction (XRD) patterns of the samples were collected at the 11-BM beamline at the Advanced Photon Source (APS) at Argonne National Laboratory using a wavelength $\lambda = 0.413742$ Å. Rietveld analysis was carried out using the General Structure Analysis System (GSAS)[31] and EXPGUI[32] for structure and phase determination. Crystal structures were visualized using VESTA.[33] Energy-dispersive X-ray spectroscopy (EDS) was performed at 20 keV in an FEI XL30 scanning electron microscope, and compositions were quantified using EDAX Genesis. Given compositions are an average over many points across the sample, and error is derived from the standard deviation of the set of measurements.

Magnetic properties were measured using a Quantum Design PPMS Dynacool equipped with a vibrating sample magnetometer (VSM) and an oven attachment for measurements over 400 K. For the field cooled magnetization (M) versus temperature (T) measurements shown, data was taken upon warming at a rate of 5 K/min under a $H = 200$ Oe field. Demagnetization factors are ignored due to sample geometry. In order to determine ΔS_M, magnetization *vs.* temperature measurements were taken on cooling at various fields from $H = 1000$ Oe to $H = 5$ kOe. According to the thermodynamic Maxwell relation,[34]

$$\left(\frac{\partial S}{\partial H}\right)_T = \left(\frac{\partial M}{\partial T}\right)_H \tag{1}$$

where S is the total entropy a material and M is the magnetization, the field-driven isothermal entropy change ΔS_M can be calculated as:

$$\Delta S_M(T, H) = \int_0^H \left(\frac{\partial M}{\partial T}\right)_{H'} \mathrm{d}H' \tag{2}$$

The smoothed M *vs.* T data were used to find the derivative $(\partial M/\partial T)$ as a function of temperature, and then integrated over field to calculate ΔS_M using Eq. 2. The smoothing is performed using Tikhonov regularization as implemented by Stickel.[35] The refrigerant capacity (RC_{FWHM}) is calculated by multiplying the peak ΔS_M by the temperature range of the full width at half maximum. Magnetization versus field (five branch hysteresis loops) were measured for the samples between +50 kOe and −50 kOe (±5 T) at 5 K and 305 K with a field sweep rate 200 Oe/s.

Spin polarized density functional theory calculations were carried out using the *Vienna ab initio simulation package* (VASP)[36] using projector augmented wave (PAW) psuedopotentials[37,38] within the Perdew-Burke-Ernzerhor (PBE) generalized gradient approximation (GGA)[39]. Spin-orbit coupling was not included. The ground state energies of all of the possible supercell orderings of Ni vacancies on Ni sites were calculated for the conventional cubic cell (x = 0, 0.25, 0.5, 0.75, and 1; 14 total cells) and for a 2×1×1 supercell of the conventional cell (x = 0.675, 0.75, and 0.875; 25 total cells). For each cell, the lattice parameters and atom positions were allowed to relax to their lowest energy state before the final energy was calculated. The structural relaxations were run iteratively until the volume change between subsequent relaxations was less than 2%. Monkhorst-Pack k-point meshes were used for all calculations with a 6×6×6 grid for the single conventional unit cells and a 4×6×6 grid for the double cells. In each case, a ferromagnetic spin arrangement was assumed, with each transition metal atom starting with a local moment of $3\mu_B$. The Python packages `pymatgen` and `custodian` were used to generate the cells and run the calculations.[40]

RESULTS AND DISCUSSION

Structural characterization

Synchrotron powder X-ray diffraction patterns are shown for the samples prepared in this study in Figure 2. In each case, a single half-Heusler (or Heusler) phase is present. No peak splitting or broadening is observed across the entire series, implying that there is no phase separation between the full and half-Heusler, in agreement with prior studies.[26–28] The full width at half maximum (FWHM) of the (220) peak (Figure 3(c)) varies negligibly across the series (± 0.0002 Å^{-1}), with no trend with respect to nickel content and no instrumental correction for broadening. The lack of a peak shoulder indicates a homogeneous distribution of nickel. This is in contrast, for example, to the case of Ni-rich TiNiSn, where a shoulder indicates an additional phase with a shifted lattice parameter corresponding to nickel interstitials.[41] The high Q-space resolution of synchrotron data can reveal peak asymmetry for a difference in lattice parameter even as small as 0.1%. There are no ferromagnetic impurities in the samples, however $<$ 2 wt% MnO is present in all samples, and $<$6 wt% of the impurity NiSb is present for the x = 0 and 0.25 samples (Table I).

In agreement with these previous studies, the lattice parameter of $MnNi_{1+x}Sb$ increases with increasing x up until the $x = 0.75$ sample, after which there is a slight decrease (Figure 3(a)). The increase in lattice parameter is consistent with the addition of nickel to the unit cell. Since this process is not a substitution, but rather a stuff-

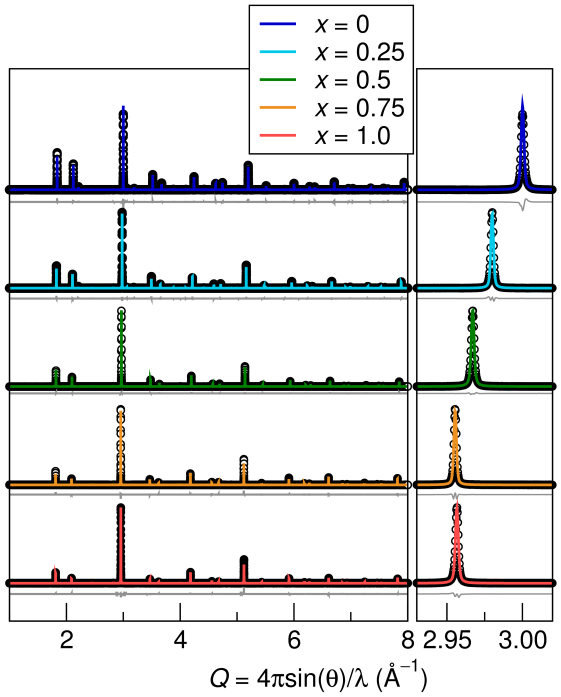

FIG. 2. Synchrotron X-ray diffraction and Rietveld refinement fits for $MnNi_{1+x}Sb$ compositions (x = 0, 0.25, 0.5, 0.75, 1.0). The enhanced view of the (220) peak shows peak shifting and a lack of peak broadening, splitting, or shouldering indicating a homogeneous addition of nickel to the unit cell rather than clustering or phase separation.

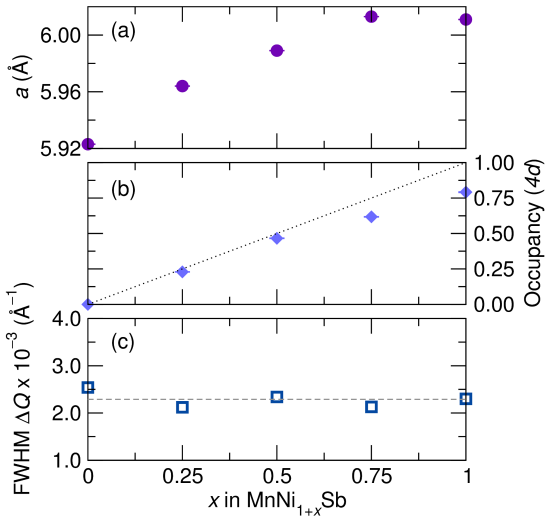

FIG. 3. (a) The lattice parameter, obtained by Rietveld refinement of synchrotron XRD, increases as nickel is added until it plateaus at a composition of $x = 0.75$. Error bars are contained within the points. (b) The refined occupancy of the $4d$ Wyckoff site (assuming a "half-Heusler like" cell) matches the nominal (dotted line) composition well for low nickel compositions, and then deviates with increasing nickel. (c) The full width at half maximum (FWHM) of the (220) peak shows very little variation across samples.

ing of atoms, it need not obey Vegard's Law. The leveling off of the lattice parameter at high nickel content, which is consistent across all previous studies,[27,28] could be due to increased disorder and non-optimal bonding.

The diffraction patterns were refined using the symmetry of the half-Heusler space group $F\bar{4}3m$, with the unit cell containing two symmetrically distinct nickel sublattices at Wyckoff positions $4c$ ($\frac{1}{4},\frac{1}{4},\frac{1}{4}$) and $4d$ ($\frac{1}{4},\frac{1}{4},\frac{3}{4}$). This unit cell allows for the half-Heusler, the full Heusler, and intermediate structures where the excess nickel can either sit on the vacant sublattice ("half-Heusler like" with nickel interstitials), or be uniformly distributed on both nickel sublattices ("Heusler like"). For the "half-Heusler like" structure, one nickel sublattice is held at 100% occupancy, and the other's occupancy is allowed to refine. These occupancies are given in Figure 3(b). For the "Heusler like" structure, the two nickel sublattices are constrained to the same occupancy, mimicking a full Heusler unit cell with vacancies randomly distributed on the one symmetrically distinct nickel site in the $Fm\bar{3}m$ space group. Rietveld refinement of all of the synchrotron XRD patterns confirms the incorporation of nickel on the $4d$ Wyckoff site ($\frac{1}{4}$, $\frac{1}{4}$, $\frac{3}{4}$), or second tetrahedral site, for compositions $x \leq 0.5$. For these compositions, R_{wp} is smaller when the occupancy of one nickel site is held at 100%, and the other is allowed to refine, as shown in Figure 4(a). For compositions $x \geq 0.75$, there is no difference (or R_{wp} is lower) when both nickel sites are constrained to the same occupancy.

To investigate this trend, and to explain why a solid solution forms in this Heusler/half-Heusler system (as opposed to, for example, $TiNi_{1+x}Sn$,[42] which phase separates), density functional theory calculations were performed. The results of calculating the energy of all of the possible orderings of the Ni vacancies on the two Ni fcc sublattices in a 1×1×1 conventional cell (12-16 atoms) are shown as filled circles in Figure 4(b). For each composition, the energies are shown relative to an interfaceless mixture of the pure Heusler and half-Heusler. The lowest energy cells form a miscibility gap with a maximum energy of 16.5 meV/atom (≈190 K) for the x=0.5 sample. This gap should be viewed as an upper limit, since enumeration of larger unit cells with more degrees of freedom would almost certainly reveal lower energy configurations of the Ni vacancies. Even considering this upper limit, the energy benefit to phase segregation is small compared to the thermal energy present during the preparation of these samples, explaining why a homogeneous solid solution is found.

For the $x = 0$, 0.25, and 0.5 cells, the orderings with one Ni sublattice completely filled and one partially empty ("half-Heusler like") are far lower in energy than orderings with vacancies spread across both sublattices ("Heusler like"). This is consistent with the Rietveld refinement preference for the half-Heusler symmetry with one filled and one partially filled Ni sublattice. The energy difference between these states is highest for the $x = 0$ case, and steadily decreases as x is increased to

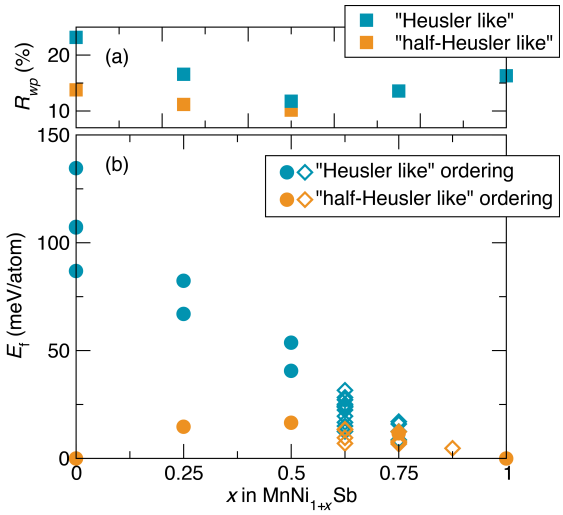

FIG. 4. (a) R_{wp} values for Rietveld refinements showing a preference for "half-Heusler like" ordering with nickel interstitials in the $4d$ Wyckoff site over the a "Heusler like" ordering with randomly distributed vacancies for low nickel compositions. For higher nickel compositions the two are indistinguishable. (b) Energies of formation relative to the phase separated mixture, from DFT, of possible configurations of Ni vacancies on the Ni sites. Orange symbols represent cells with all of the Ni vacancies on only one of the two FCC sublattices ("half-Heusler like"), while blue symbols represent cells with Ni vacancies on both sublattices ("Heusler like"). In each case, the filled round symbols indicate orderings within a single conventional cell, while the empty diamond symbols indicate orderings within a $2\times1\times1$ supercell (only calculated for $x >$). These calculations suggest a small miscibility gap of less than 16.5 meV/atom, with a preference for half-Heusler like symmetry (complete occupation of one Ni sublattice) for $x \leq$0.5 only.

0.5. For the $x = 0.75$ case, there is only one $1\times1\times1$ ordering (half-Heusler like), so the $2\times1\times1$ orderings were calculated for $x = 0.625$, 0.75, and 0.875. Again, the half-Heusler like cells tend to be the lowest in energy, but the gap between these cells and the Heusler like cells has dropped to $<$5 meV/atom. Therefore, in samples prepared at finite temperature, both types of symmetries are expected to be present, consistent with the synchrotron X-ray diffraction refinements.

Rietveld refinement also reveals a less-than-nominal site occupancy for nickel at higher nickel compositions. The refined occupancy of the second tetrahedral nickel site is given in Figure 3(b), assuming a "half-Heusler like" ordering. While the refined occupancy matches the nominal occupancy well for low nickel contents, it starts to deviate for $x = 0.5$, and then deviates more severely for $x = 0.75$ and 1.0 samples. This can be explained by anti-site defects, where some Ni occupies the Mn site due to an Mn deficiency from processing. Anti-site defects between the X and Y atoms of Heuslers are very common,

TABLE I. Relevant physical properties obtained from Rietveld refinement of synchrotron powder XRD. Occupancy refers to the fractional occupancy of the $4d$ Wyckoff site, or second tetrahedral nickel site.

x	a (Å)	Occ. ($4d$)	R_{wp} (%)	Impurities (wt%)
0.00	5.9234(1)	0.0	13.78	MnO [0.6(1)]
				NiSb [5.0(1)]
0.25	5.9634(1)	0.229(1)	11.16	MnO [1.60(2)]
				NiSb [4.30(2)]
0.50	5.9895(1)	0.466(2)	10.15	MnO [1.5(2)]
0.75	6.0130(1)	0.618(2)	13.57	MnO [1.7(4)]
1.00	6.0106(1)	0.792(3)	16.29	MnO [3.1(8)]

and the formation energy of these defects in the Mn-Ni-Sb compounds is low.[24]

While, to the best of our knowledge, no ternary phase diagram is available for this compound, deviations from the nominal composition are expected to be accomodated by the formation of other intermetallic phases, as is observed in many other systems. In the half-Heusler, the loss of Mn to the MnO impurity and during processing is compensated by the formation of NiSb. The phase fraction of NiSb reveals that about 15 at% of Mn is lost during processing. As x increases, NiSb no longer forms to compensate the loss of Mn. Instead, the excess nickel occupies the empty Mn site rather than the $4d$ Wyckoff site, leading to a lower occupancy of Ni sites than expected from the nominal composition. For this reason, we obtain a Heusler structure with some Ni on the Mn site, and no NiSb impurity phase. It is difficult to distinguish Ni on the Mn site and *vice versa* due to their similar X-ray scattering cross sections. Elemental analysis of the full Heusler by EDS gives a composition of $Mn_{0.88(1)}Ni_{2.01(1)}Sb$, indicating an overall loss of manganese in close agreement with the Rietveld analysis. This analysis also confirms that the nickel is incorporated into the sample, and so it must sit on these empty manganese sites if the nickel sites are less than fully occupied. This will in turn influence the magnetic properties, since manganese holds the moment.[7,24,43]

Magnetic characterization

The decrease in transition temperature with increasing nickel can be seen from Figure 5(a), which shows magnetization as a function of temperature for each composition. This trend in T_C is further illustrated in Figure 6(b). Values for magnetization data are listed in Table II. Tunable magnetic transition temperatures are important for engineering magnetic refrigeration and thermomagnetic power generation devices. Varying Ni content has a much stronger effect on the Curie temperature than varying the Mn:Z ratio.[7,16,44,45]

The Heusler and half-Heusler endmembers are ex-

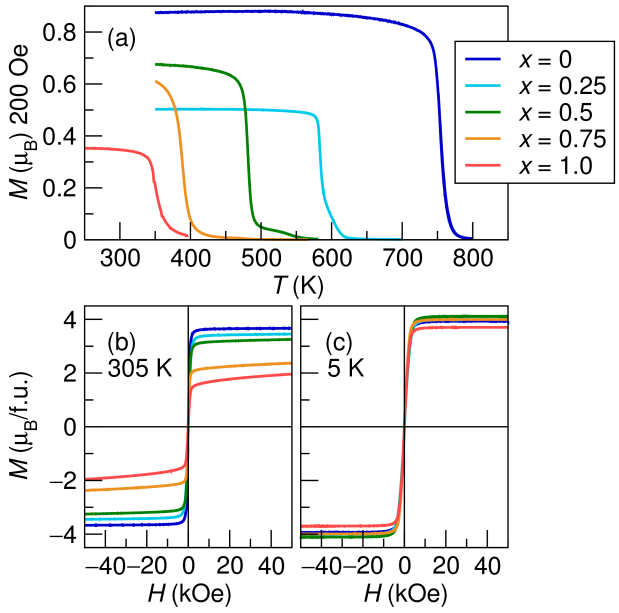

FIG. 5. (a) Magnetization *vs.* temperature showing the ferromagnetic to paramagnetic transition of each sample under a 200 Oe field (b) Magnetization *vs.* applied field at 305 K shows a decreasing saturation magnetization as more nickel is incorporated into the structure. (c) M *vs.* H at 5 K reveals a maximum magnetization per formula unit for intermediate compositions.

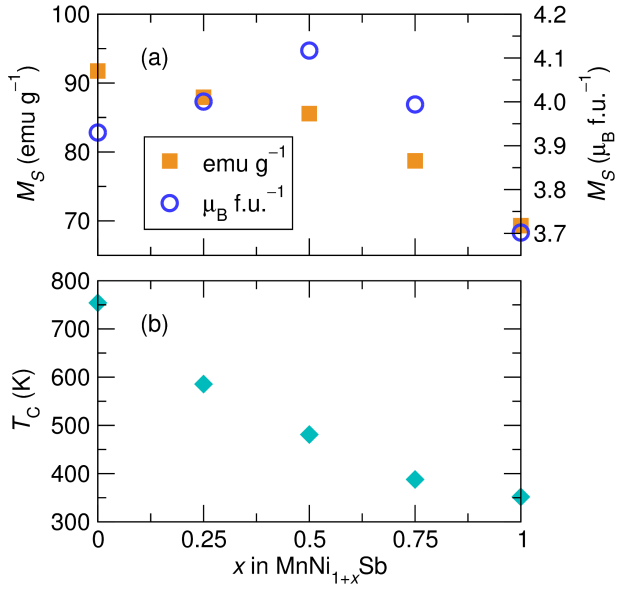

FIG. 6. (a) Saturation magnetization at 5 K per formula unit (f.u.) and in gravimetric units. The moment per formula unit reaches a maximum at $x = 0.5$. (b) The Curie temperature decreases significantly with the addition of nickel, and is tunable over a wide range by adjusting x.

TABLE II. Magnetic properties across the series. RC refers to RC_{FWHM}, the refrigerant capacity calculated by multiplying peak ΔS_M by the full width at half maximum.

x	M_S (5 K)		T_C (K)	ΔS_M (J/kg K)		RC (J/kg)
	(μ_B/f.u.)	(emu/g)		2 T	5 T	
0	3.93	91.75	754	−1.49	−2.93	196
0.25	4.00	87.95	586	−1.25	−2.40	220
0.5	4.12	85.57	481	−1.12	−2.29	245
0.75	3.99	78.71	388	−0.68	−1.48	262
1.0	3.70	69.35	352	−0.58	−1.35	235

pected to be soft ferromagnets, which is consistent with the lack of hysteresis in the magnetization data (Figure 5(b) and (c)). The intermediate compositions also show no hysteresis despite a changing magnetic interaction, from RKKY-like interactions in the Heusler to localized interactions in the half-Heusler.[26] This data was used to extract the saturation magnetization at 5 K.

The saturation magnetization per formula unit reaches a maximum at $x = 0.5$ (Figure 6(a)), in agreement with previous reports.[27,28] The moment in these samples is carried by the manganese, and so the addition of nickel changes the atomic weight, and therefore overall moment, without having a large effect on the local Mn moment.[43] The addition of nickel affects the interactions between magnetic Mn atoms by modifying interatomic distance and electronic structure, as described by Rusz *et al.*[26,43] However, both the gravimetric moment and ΔS_M decrease monotonically as x increases.

The magnitude of the magnetocaloric effect can be described by the entropy change induced by the isothermal application of a magnetic field, $\Delta S_M(H,T)$. Since this is dependent on $(\partial M/\partial T)$, the peak value will occur at the Curie temperature, where magnetization changes rapidly with temperature. Experimentally, magnetization is measured as a function of temperature at a variety of fields, shown in Figure 7(a). $\Delta S_M(H,T)$ is calculated according to Eq. 2 by taking the derivative, $(\partial M/\partial T)$, and integrating with respect to field, shown in Figure 7(b) and (c).

ΔS_M as a function of temperature is given for several magnetic field strengths in Figure 8. The absolute value of ΔS_M decreases and the curve broadens as x increases. For intermediate compositions, specifically increasing nickel content from $x = 0.25$ to $x = 0.5$, there is a 90 K change in transition temperature, while ΔS_M decreases less than 5%, from 2.40 J kg^{-1} K^{-1} to 2.29 J kg^{-1} K^{-1} at $H = 5$ T. This is accompanied by a broadening of the ΔS_M curve, which increases the usable temperature range, or full width at half maximum (FWHM), of the material. The product of the FWHM and the peak ΔS_M yields the refrigerant capacity (RC).[2] While the magnitude of ΔS_M decreases as x increases,

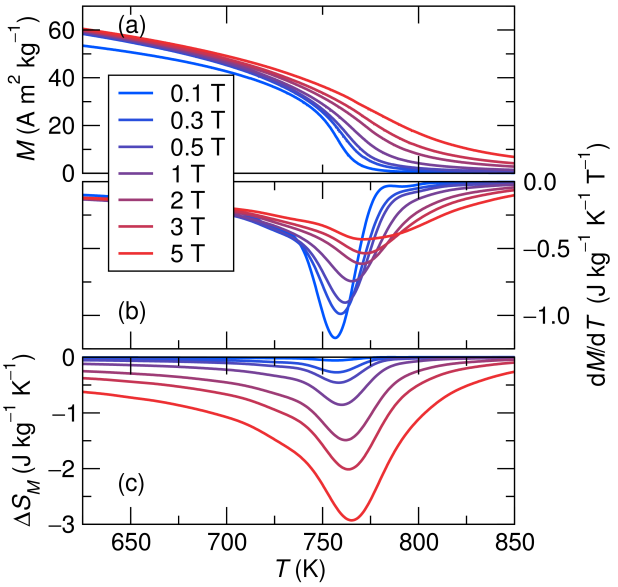

FIG. 7. Measurements of MnNiSb are shown. (a) Magnetization *vs.* temperature measurements are taken at various fields. These curves are fitted, and the derivative is shown in (b). The derivative is integrated over field according to Eq. 2, which is derived from Maxwell relations, to give the isothermal entropy change ΔS_M shown in (c).

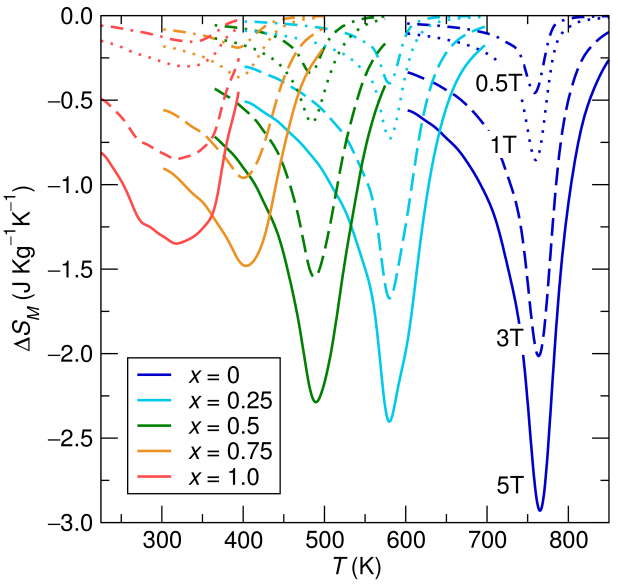

FIG. 8. The absolute value of ΔS_M decreases and broadens with increasing nickel concentration. However, for $x = 0.25$ to $x = 0.5$ there is a large shift in transition temperature (90 K) without a significant decrease in ΔS_M.

the broadening of the transition leads to an increase in the refrigerant capacity with a maximum at $x = 0.75$. The structure in the ΔS_M curve for $x = 1$ is likely an artifact associated with fitting the derivatives of a the very broad magnetic transition, or may be due to small amounts of inhomogeneity in that sample.

While M_S is often used as an indicator for the magnetocaloric effect, in this case it is misleading to compare the moment per formula unit to the gravimetric ΔS_M. Rusz *et al.* reports that the half-Heusler displays localized (exponentially damped) exchange interactions, while the full Heusler displays longer range oscillatory RKKY-like interactions.[26] The localized interactions in the half-Heusler are more strongly coupled to the structure, such that there is a more abrupt change in magnetization at T_C. The extension of magnetic interactions to longer range corresponds to lessened magnetostructural coupling and a broader magnetic transition, leading to a smaller $|\Delta S_M|$ as x increases. This is consistent with our prior work,[25] which suggests the coupling between magnetism and structure is important to ΔS_M, as evidenced by the correlation with the magnetic deformation (Σ_M) parameter.

CONCLUSIONS

The increase in magnitude of ΔS_M with decreasing x in $MnNi_{1+x}Sb$ was successfully predicted using a DFT-based proxy, the magnetic deformation Σ_M. This suggests the magnetovolume coupling, which is stronger in the half-Heusler due to localized magnetic interactions, plays a large role in determining ΔS_M. Decreasing nickel content increases magnetization, reduces broadening of the magnetization with temperature, and overall increases $|\Delta S_M|$ in these compounds. This is useful to incorporate into studies of off-stoichiometric Heuslers ($Mn_{1+x}Ni_2Z_{1-x}$), which vary the Mn-Z ratio while keeping the full Heusler structure. We have demonstrated versatile tuning of Curie temperature, and values for $|\Delta S_M|$ are comparable to or smaller than similar $MnNi_2Z$ Heuslers with second-order transitions such as $MnNi_2Sn$, with a $\Delta S_M = -2.1$ J/Kg K, or $Mn_{1.4}Ni_2In_{0.6}$ with $\Delta S_M = -6.3$ J/Kg K for $\Delta H = 5$ T.[7,25] While the operation temperature of the $MnNi_{1+x}Sb$ solid solution is high for applications in magnetic refrigeration, this study provides a materials system with a range of transition temperatures for thermomagnetic energy generation. These materials may be useful in converting low and medium grade waste heat to electricity.[3]

ACKNOWLEDGMENTS

The research reported here was supported by the Materials Research Science and Engineering Center at UCSB (MRSEC NSF DMR 1720256) through IRG-1. J.D.B. is supported by the National Science Foundation Graduate Research Fellowship Program by Grant 1650114. Use of the Shared Experimental Facilities of the Materials Research Science and Engineering Center at UCSB (MRSEC NSF DMR 1720256) is gratefully acknowledged. The UCSB MRSEC is a member of the NSF-supported Materials Research Facilities Network (www.mrfn.org). We

also acknowledge support from the Center for Scientific Computing at UCSB, from the California NanoSystems Institute, the UCSB MRSEC (DMR-1720256) and NSF CNS-0960316. Use of the Advanced Photon Source at Argonne National Laboratory was supported by the U.S. Department of Energy, Office of Science, Office of Basic Energy Sciences, under Contract No. DE-AC02-06CH11357.

* emilylevin@mrl.ucsb.edu

[1] G. V. Brown, J. Appl. Phys. **47**, 3673 (1976).
[2] V. Franco, J. S. Blazquez, B. Ingale, and A. Conde, Annu. Rev. Mater. Res. **42**, 305 (2012).
[3] R. A. Kishore and S. Priya, Sustainable Energy Fuels **1**, 1899 (2017).
[4] K. Kamiya, H. Takahashi, and T. Numazawa, Cryocoolers **14**, 637 (2007).
[5] Y. Song, C. Leighton, and R. D. James, in *Heusler Alloys*, Vol. 222, edited by C. Felser and A. Hirohata, pp. 269–291.
[6] O. Gutfleisch, T. Gottschall, M. Fries, D. Benke, I. Radulov, K. P. Skokov, H. Wende, M. Gruner, M. Acet, P. Entel, and M. Farle, Phil. Trans. R. Soc. A **324**, 20150308 (2016).
[7] S. Singh, L. Caron, S. W. D. Souza, T. Fichtner, G. Porcari, S. Fabbrici, C. Shekhar, S. Chadov, M. Solzi, and C. Felser, Adv. Mater. **28**, 3321 (2016).
[8] R. A. de Groot, F. M. Mueller, P. G. van Engen, and K. H. J. Buschow, Phys. Rev. Lett. **50**, 2024 (1983).
[9] I. Galanakis, P. Mavropoulous, and P. H. Dederichs, J. Phys. D: Appl. Phys. **39**, 765 (2006).
[10] K. Ullakko, J. K. Huang, C. Kantner, R. C. O'Handley, and V. V. Kokorin, Appl. Phys. Lett. **69**, 1966 (1996).
[11] Y. Sutou, Y. Imano, N. Koeda, T. Omori, R. Kainuma, K. Ishida, and K. Oikawa, Appl. Phys. Lett. **85**, 4358 (2004).
[12] S. J. Murray, M. Marioni, S. M. Allen, R. C. O'Handley, and T. A. Lograsso, Appl. Phys. Lett. **77**, 886 (2000).
[13] S. Aksoy, T. Krenke, M. Acet, E. F. Wasserman, X. Moya, L. Mañosa, and A. Planes, Appl. Phys. Lett. **91**, 241916 (2007).
[14] A. Aliev, A. Batdalov, S. Bosko, V. Buchelnikov, I. Dikshtein, V. Khovailo, V. Koledov, R. Levitin, V. Shavrov, and T. Takagi, J. Magn. Magn. Mater. **272–276**, 272 (2004).
[15] V. Basso, C. P. Sasso, K. P. Skokov, O. Gutfleisch, and V. V. Khovaylo, Phys. Rev. B **85**, 014430 (2012).
[16] J. Du, Q. Zheng, W. J. Ren, W. J. Feng, X. G. Liu, and Z. D. Zhang, J. Phys. D: Appl. Phys. **40**, 5523 (2007).
[17] T. Krenke, E. Duman, M. Acet, E. F. Wassermann, X. Moya, L. Mañosa, and A. Planes, Nat. Mater. **4**, 450 (2005).
[18] A. Planes, L. Man, X. Moya, T. Krenke, M. Acet, and E. F. Wassermann, J. Magn. Magn. Mater. **310**, 2767 (2007).
[19] E. Stern-Taulats, P. O. Castillo-Villa, L. Mañosa, C. Frontera, S. Pramanick, S. Majumdar, and A. Planes, J. Appl. Phys. **115**, 173907 (2014).
[20] T. Gottschall, K. P. Skokov, B. Frincu, and O. Gutfleisch, Appl. Phys. Lett. **106**, 021901 (2015).
[21] T. Gottschall, K. Skokov, R. Burriel, and O. Gutfleisch, Acta Mater. **107**, 1 (2016).
[22] J. Liu, T. Gottschall, K. Skokov, J. D. Moore, and O. Gutfleisch, Nat. Mater. **11**, 620 (2012).
[23] T. Fichtner, G. Kreiner, S. Chadov, G. H. Fecher, W. Schnelle, A. Hoser, and C. Felser, Intermetallics **57**, 101 (2015).
[24] B. Alling, S. Shallcross, and I. A. Abrikosov, Phys. Rev. B **73**, 064418 (2006).
[25] J. D. Bocarsly, E. E. Levin, C. A. Garcia, K. Schwennicke, S. D. Wilson, and R. Seshadri, Chem. Mater. **29**, 1613 (2017).
[26] J. Rusz, J. Kudrnovsky, and I. Turek, J. Magn. Magn. Mater. **310**, 1654 (2007).
[27] P. J. Webster and R. Mankikar, J. Magn. Magn. Mater. **42**, 300 (1984).
[28] J. Schaf, L. M. Zelis, E. R. Fraga, R. P. Livi, F. C. Zawislak, P. J. Webster, and R. M. Mankikar, Hyperfine Interact. **4**, 397 (1978).
[29] K. J. Rao, B. Vaidhyanathan, M. Ganguli, and P. A. Ramakrishnan, Chem. Mater. **11**, 882 (1999).
[30] C. S. Birkel, J. E. Douglas, B. R. Lettiere, G. Seward, N. Verma, Y. Zhang, T. M. Pollock, and R. Seshadri, Phys. Chem. Chem. Phys. **15**, 6990 (2013).
[31] A. C. Larson and R. B. Von Dreele, Los Alamos Natl. Lab. [Rep.] LA (U.S.) , 86 (2000).
[32] B. H. Toby, J. Appl. Crystallogr. **34**, 210 (2001).
[33] K. Momma and F. Izumi, J. Appl. Crystallogr. **44**, 1272 (2011).
[34] V. K. Pecharsky and K. A. Gschneidner, J. Magn. Magn. Mater. **200**, 44 (1999).
[35] J. J. Stickel, Comput. Chem. Eng. **34**, 467 (2010).
[36] G. Kresse and J. Furthmüller, Phys. Rev. B **54**, 11169 (1996).
[37] P. E. Blöchl, Phys. Rev. B **50**, 17953 (1994), arXiv:arXiv:1408.4701v2.
[38] G. Kresse and D. Joubert, Phys. Rev. B **59**, 1758 (1999).
[39] J. P. Perdew, K. Burke, and M. Ernzerhof, Phys. Rev. Lett. **77**, 3865 (1996).
[40] S. P. Ong, W. D. Richards, A. Jain, G. Hautier, M. Kocher, S. Cholia, D. Gunter, V. L. Chevrier, K. A. Persson, and G. Ceder, Comput. Mater. Sci. **68**, 314 (2013).
[41] J. E. Douglas, P. A. Chater, C. M. Brown, T. M. Pollock, and R. Seshadri, J. Appl. Phys. **116**, 163514 (2014).
[42] J. E. Douglas, C. S. Birkel, M. Miao, C. Torbet, G. D. Stucky, T. M. Pollock, and R. Seshadri, Appl. Phys. Lett. **101**, 183902 (2012).
[43] J. Rusz, L. Bergqvist, J. Kudrnovsky, and I. Turek, Phys. Rev. B **73**, 214412 (2006).
[44] T. Gottschall, K. P. Skokov, D. Benke, M. E. Gruner, and O. Gutfleisch, Phys. Rev. B **93**, 184431 (2016).
[45] M. Khan, N. Ali, and S. Stadler, J. Appl. Phys. **101**, 053919 (2007).